Applied Energy 301 (2021) 117473

Contents lists available at ScienceDirect

Applied Energy

journal homepage: www.elsevier.com/locate/apenergy

A global integral terminal sliding mode control based on a novel reaching law for a proton exchange membrane fuel cell system

Cristian Napole *, Mohamed Derbeli, Oscar Barambones

Engineering School of Vitoria, Basque Country University (UPV/EHU), Nieves Cano 12, Vitoria Gasteiz, 01010, Álava, Spain

GRAPHICAL ABSTRACT

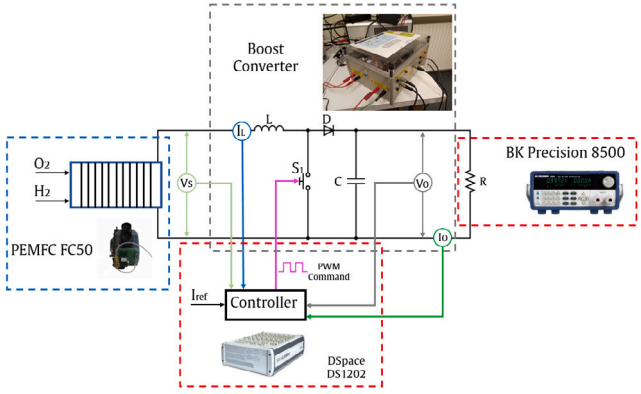

ARTICLE INFO

MSC:
0000
1111

Keywords:
PEMFC
Boost-converter
Sliding mode control
Global integral terminal sliding mode control
Quick reaching law

ABSTRACT

Proton exchange membrane fuel cells are devices with huge potential for renewable and clean industries due to their high efficiency and low emissions. Since the proton exchange membrane fuel cell employed in this research supplied a low output voltage, it was encouraged to use a boost converter with a designed non-linear controller to provide a suitable end-user voltage. In this paper, we proposed a novel control framework based on sliding mode control, which is a global integral sliding mode control linked with a quick reaching law that has been implemented in a commercial fuel cell system Heliocentris FC50 through a dSpace 1102 control board. We compared the strategy with a conventional sliding mode controller and an integral terminal sliding mode controller where we addressed a Lyapunov stability proof has for each structure. We contrasted the experimental outcomes where we proved the superiority of the proposed novel design in terms of robustness, convergence speed. Additionally, as the sliding mode controllers are well known by the energy consumption caused by the chattering effect, we analysed every framework in these terms. Finally, it was found that the proposed structure offered an enhancement in the energy consumption issues. Moreover, the applicability of the proposed control scheme has been demonstrated through the real time implementation over a commercial fuel cell.

1. Introduction

In recent years, hydrogen power generation captured the interest of the research community since the H_2 can reach an energy density value of 120 MJ/kg which is almost 5 times higher compared to the coal [1]. Regarding production costs, the target had been reduced from 4.2USD in 2015 and aimed to be 1.7USD in 2020 [2]. The electrochemical conversion of hydrogen as a gas into useful electricity can be achieved through fuel cells, devices that drew the attention since they

* Corresponding author.
E-mail address: cristianmario.napole@ehu.eus (C. Napole).

https://doi.org/10.1016/j.apenergy.2021.117473
Received 22 March 2021; Received in revised form 9 July 2021; Accepted 15 July 2021
Available online 5 August 2021

were discovered by William Grove in 1839 [3]. Thenceforth, the attractiveness of fuel cells represents a trend in research as it is expected that this technology could reach its maturity near 2030 [4]. Additionally, because of the groundbreaking innovation of fuel cell electric vehicles (FCEV) and large capacity stationary fuel cells (LCSFC), the interest has been growing exponentially since 2007 [5]. This is principally due to their emissions level that could reach 0% (depending on the type of fuel) [6]; besides, the efficiency can yield up to 60% [7]. Despite that an assorted variety of fuel cells had been developed, proton exchange membrane fuel cells (PEMFC) had a significant enhancement in recent years [8]. The production costs not only provided a downsizing feature but also a performance improvement which covers high energy density and robustness [9]; thus, it has been a matter of research for several applications like transport vehicles [10]. PEMFC performance can be increased through the control of diverse variables such as air–fuel flow to obtain an appropriate temperature and output voltage [11]. Nevertheless, drawbacks of this strategy are related to risks (manipulation of hydrogen), external factors and maintenance [12]. Additionally, if the output voltage is unsuitable for end-user purposes, a power electronic converter with an integrated designed controller is required to be link to the PEMFC [13]; in this manner, an increment of the system performance is also achieved.

Linear controllers can be a suitable initial option to control a DC–DC converter. Hence, a typical first and classic approach like a proportional–integral–derivative (PID) has been implemented several times in a DC–DC boost converters. A striking aspect has been accomplished in the research conducted by the authors of [14] where they compared controller tuning strategies in simulation environments. Procedures like Ziegler–Nichols, Chien–Hrones–Reswick and online optimization achieved respectively, 11.8%, 17.1% and 2.16% of overshoot reduction. Diversely, an advance linear structure used in boost converters control is μ-synthesis approach as it was developed in the investigation of [15]. In that work, simulations were performed with the robust strategy and compared with a PI controller where further reduction of overshoot was observed along a step function. On the other hand, a classic linear quadratic regulator (LQR) strategy has been proposed for a PEMFC in [16] where the maximum overshoot reached 96.21%. However, a main drawback of these analysed studies is that simulation results were provided. Actually, boost converters are mainly nonlinear due to the switching states and device perturbations which limits the implementation of linear controllers [17].

A nonlinear strategy design can improve the effectiveness, especially when a real-time controller is embedded [18]. Fuzzy-logic controller (FLC) represents a non-linear strategy which its construction is based on the designer expertise within the system and traduced through if-then causal rules in fuzzy sets. FLC is known for its simplicity and robustness which are the main advantages when it is employed in complex models [19]. For instance, the authors of [20] used an adaptive FLC strategy for a boost converter linked to a PEMFC where simulations were carried and a final experiment was performed: results showed the chattering amplitude reached 2.4 V in the real device outcomes. However, the implementation of FLC has a significant drawback when complex strategies are required; the fuzzy-set growth implies that the computational requirements need to increment as well [21]. Another nonlinear controller is back-stepping (BSTP) which is a Lyapunov-based design that intents to split the whole feedback-system into sub-systems with the aim of developing a controller that considers the sub-parts [22]. Therefore, the mechanics of this approach through a Lyapunov-design can ensure the stability of the entire close-loop system. In [23], the researchers implemented a BSTP to control a boost converter where the aim was to track the maximum power point (MPP) and an improvement of 12% was shown. Recently, an advance implementation included a neural adaptive BSTP controller, and it was embedded in a boost converter for voltage regulation where an overshoot of 11.6% with low settling time was achieved [24]. Nevertheless, BSTP drawbacks are associated to its complex design since an advance Lyapunov analysis is involved to reach a suitable control law [25]; in addition, the robustness is limited because of its sensibility to uncertainties and disturbances [26]. These issues can be counteracted with globally linearizing control (GLC) combined with adaptive state observer (ASO), which was presented in 2018 [27]; however, results showed several discrepancy in the obtained model. Model predictive control (MPC) is another non-linear approach that explicitly uses a plant model to calculate an optimal control action subject to constraints on actuation and states [28]. The study made by the authors of [29] showed the design and implementation of an MPC in a hardware in the loop (HIL) where a boost converter was emulated for voltage tracking. Despite that the error was enough reduced, the computational resources were one of the main highlights because a leading disadvantage of MPC are the requirements over low cost processors [30].

Sliding mode control (SMC) is a nonlinear controller which main advantage over previously described tools is that it provides a prompt response, robustness, stability in undetermined environments and low computation is required [31]. This technique gathers a control law that changes the dynamics of a system based on a sliding surface that ensures the convergence [32]. Nevertheless, a severe deficiency of this strategy is the infinite time in which the states can achieve the equilibrium [33]. Consequently, in 1988, the terminal sliding mode control (TSMC) was introduced like a terminal attractor [34], and then as a control strategy in 1993 by Gulati and Venkataraman [35] where they aimed to achieve a finite time response. Despite this mentioned advantage, the TSMC is still slow when the system states are distant from the origin and singularities were found which could yield to an unbounded control signal [36]. An option proposed to counter the singularity problem is using high order sliding mode control (HOSMC); traditionally, it is also used to reduce the chattering, which represents an ordinary feature of SMC because it generates an increment in the energy consumption. Regardless the advantages of the HOSMC, the main issues are related to: complex stability proof [37] and it requires high order derivatives which can increase the noise in a feedback loop [38]. Integral terminal sliding mode control (ITSMC) is a composed approach that not only improves the time convergence but also enhances the chattering avoidance properties and the system dynamics [39]. For instance, authors of [40] used an ITSMC for a hybrid AC/DC grid where the comparison against SMC showed an enhancement in terms of performance and robustness. In regards to the implementation in converters, it was uncovered that a fractional ITSMC was designed and embedded in a buck converter type where the outcomes showed an improvement of time convergence even with unknown uncertainties [41]. Another recent developed scheme is the usage of global terminal sliding mode control (GTSMC) with quick reaching law (QRL) [42]; this combines the benefits of TSMC with the global strategy that includes a linear design and pretends the system to reach an equilibrium in a limited time [43]. The QRL is entrenched to reduce the chattering at a cost of shrinking the reaching speed [42].

As ITSMC was tested in converters where the performance was enhanced, the energy consumption of the chattering and rate response can still be improved [44]. Therefore, the innovation of this research paper is the usage of a global integral terminal sliding mode control (GITSMC) combined with a QRL in a boost converter for a commercial PEMFC. As it was analysed, a fair comparison is against SMC but also the use of ITSMC is advantageous to achieve intriguing progressive results. This is an innovative contrast and implementation since as we had investigated, the employment of GITSMC with QRL in a real boost-converter with PEMFC has never been analysed. Moreover, derived on the proposed combination, we expected a reduction in energy consumption as an approach based on ITSMC was implemented and as previously mentioned, it is known for its chattering lessening features.

We arranged the structure of this paper as follows. A description of the hardware used is detailed in Section 2. The design of the controllers is analysed in details within their stability proofs in Section 3. The experimental outcomes of the controllers implementation are presented in Section 4 and a summarize of the work produced is provided in Section 5.

Table 1
PEMFC technical data.

Fuel cell features		Electrical features	
Type	Heliocentris FC-50W w/10 cells	Operating Voltage	2.5–9 VDC
Cooling	Cooling fan	Operating Current	0–10 A
Fuel	H_2	Rated power output	40 W
Dimensions	$12 \times 10.3 \times 13.5$ cm	Max. output power	50 W
Weight	1150 g	Open-circuit voltage	9 VDC
H_2 Flowmeter		1.5 MPa Kit	
Precision	0.8% of the quantified value	Inlet pressure	0.1–1.5 MPa
Measuring range	10–1000 sml/min	Outlet pressure	0.06 MPa
Thermal		H_2 20 MPa kit	
Operating temperature	15–50 °C	Inlet pressure	20 MPa
Max. start temperature	45 °C	Outlet pressure	0.1–1.5 MPa
Fuel		H_2 Detector	
Recommended H_2 purity	5.0 (99.999%)	Type of sensor	H_2 4%
H_2 input pressure	0.04–0.8 MPa	Measuring principle	3 electrode sensor
H_2 consumption	Max. 700 sml/min (at 0 °C, 101.3 MPa)	Range	0–4%

Table 2
TEP-192.

Parameter	Value
Inductance	6 μH
Input capacitor	1500 μF
Output capacitor	3000 μF
Max. switching frequency	20 kHz
Max. input voltage	60 V
Max. input current	30 A
Max. output voltage	250 V
Max. output current	30 A

2. Hardware description

Experiments were based on a real-time platform with the aim to tuning the controllers so as to achieve the best performance. We used a Heliocentris PEMFC PEM FC50 stack with 10 cells connected in series where each one has an effective membrane of 25 cm^2 and a thickness of 175 μm while the electrodes have 0.3 $mg.Pt/cm^2$ of platinum. The cells bundle can generate up to 5 VCC with a current rate of 8–10 A and produce more than 40 W. We fed the PEMFC with high purity hydrogen which can reach up to 99.999 vol% from a compressed cylinder at 1 MPa. Because the device is commercial and to provide enough security to the system, the fuel supply is controlled by an integrated control board which also manages two fans that are responsible for the oxygen, membrane humidity and temperature. In this sense, this embedded controller not only helps in the chemical transformation and refrigeration but also prevents over-loads and short circuits. Further technical details of the PEMFC are enlisted in Table 1.

The boost converter is a TEP-192, which technical information is summarized in Table 2. As operators, we could control the metal–oxide–semiconductor-field-effect transistor (MOSFET) with a switching input (that can reach up to 20 kHz) originated from a PWM device generator.

We used a dSpace MicroLabBox DS1202 as a PWM generator since this device is a flexible and reliable hardware frequently involved in mechatronics research as it is also robust with high performance. It consists of 100 channels for input/output signals which can be configured as analogue, digital or PWM. Inside this instrument, there is a programmable FPGA with a dual-core processor which clock is able to reach up to 2 GHz. Furthermore, it supports Real-Time-Interface (RTI) which is a platform that allows a C-code generation into the DS1202 in a fast and automatic way so that the designer could concentrate only in the development of the Simulink interface. The DS1102 is managed through ControlDesk, a software by dSpace which not only shows the acquired and records the data in real-time but also grants the possibility to tune parameters previously settled in Simulink. Additionally, the experiments that we conducted for the current research showed that the DC/DC boost converter delivers excessive noise in the signals at the analogue–digital channel (ADC). Therefore, we implemented low-pass filters during the data acquisition with the aim of achieving suitable and legible signals.

Finally, we closed the circuit through the usage of a programmable load BK Precision 8500. This is a single output resistance for DC loads which grants a shift between 0.1 up to 1000 Ω. Regarding to the power allowed, it can endure up to 120 W at which the input voltage should not be higher than 115 V at 47 Hz. The described hardware system is shown in Fig. 1.

3. Control design

The prime objective is to follow a specific current reference named as I_{ref} through a comparison of three types of controllers: SMC, ITSMC and GITSMC combined with QRL. Certainly, the robustness and a suitable control signal needed to be accomplished to achieve an acceptable performance of the proposed strategies. Therefore, for further calculations, we define the error as e such that the I_{ref} is the reference current.

$$e = I_L - I_{ref} \tag{1}$$

Fig. 1 shows the equivalent electric circuit which consists of an inductor (L), a diode (D), switching device (S_1), a capacitor (C) and a load (R). The device S_1 generates a pulse width modulation (PWM) signal that switches between ON and OFF so as to adjust the voltage. The relation between the stack voltage (V_s) and the output voltage (V_o) is expressed through the duty cycle d. This implies that when the duty cycle increases, the output voltage follows a consistent trend. The mechanics that involves d within the boost converter is governed by a controller which sends a PWM signal to the switching element and the states of the circuit shift in two different configurations which aim to the following state space representation.

$$\begin{cases} \begin{bmatrix} \frac{di_L}{dt} \\ \frac{dV_o}{dt} \end{bmatrix} = \begin{bmatrix} 0 & \frac{-(1-d)}{L} \\ \frac{(1-d)}{C} & -\frac{1}{RC} \end{bmatrix} \cdot \begin{bmatrix} i_L \\ V_o \end{bmatrix} + \begin{bmatrix} \frac{1}{L} \\ 0 \end{bmatrix} V_s \\ y = \begin{bmatrix} 0 & 1 \end{bmatrix} \cdot \begin{bmatrix} i_L \\ V_o \end{bmatrix} \end{cases} \tag{2}$$

The general control law expression, according to the design procedure of a sliding controller [45], is composed by an equivalent term (u_{eq}) which intention is to bring the system to the sliding surface and a switching term (u_{sw}) that preserves the system in the surface. The latter described also takes into account that the preservation implies to quell

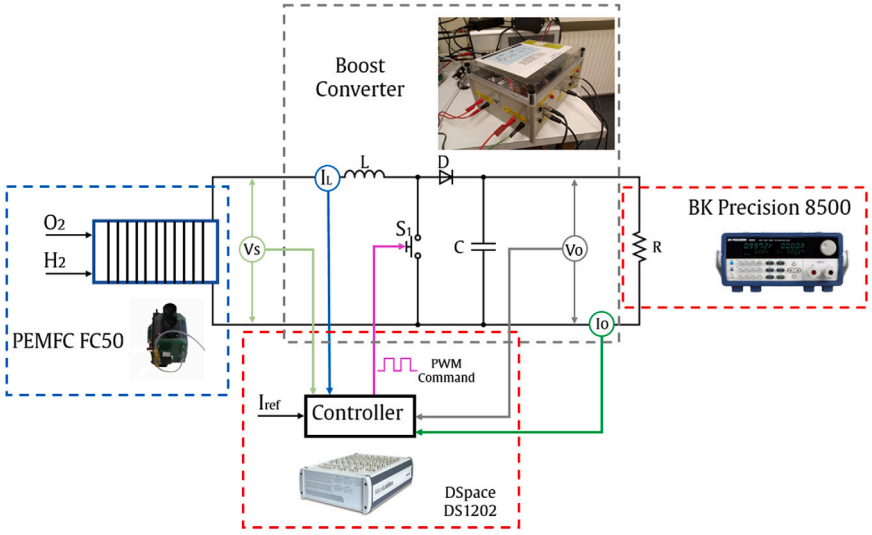

Fig. 1. System and implementation description for the hardware and control design between the PEMFC, boost converter, DS1202 and BK Precision 8500.

disturbances, unknown dynamics, etc. These two can be translated mathematically as:

$$u = u_{eq} + u_{sw} \tag{3}$$

Since all the involved controllers have parameters to be tuned, we used the same strategy for each. Hence, we employed as a performance index the integral of the absolute error (IAE) which had to be minimum. This is expressed through Eq. (4) which was implemented and where e_i is the error at the ith sample, Δt is the sampling time and N is the number of samples used. Simultaneously, the control signal was inspected in the pursuit of a suitable performance.

$$IAE = \sum_{i=1}^{N} |e_i| \Delta t \tag{4}$$

3.1. Conventional sliding mode control

A first step in the design of a SMC is to choose an adequate surface; in our case, we followed the suggestions that the authors of [46] who defined a suitable expression related on the dynamics of the system and yields the variables to be control at a reference value.

$$S_1 = \left(\frac{d}{dt} + \lambda\right)^{r-1} e \tag{5}$$

The former expression has the constants r and λ which are, respectively, the relative degree of the system and a positive constant associated with the bandwidth of the control to be designed [47]. Previously, we showed that the system is a second order type and thus, $r = 2$. Hence, the surface can be expressed by (6).

$$S_1 = \dot{e} + \lambda e \tag{6}$$

Using (2), (1) and (3), the surface derivative can be expressed as the following (7).

$$\dot{S}_1 = \frac{V_o}{L} u - \frac{V_o}{L} + \frac{V_s}{L} + \lambda \cdot e \tag{7}$$

As we previously enacted, (3) refers to two terms that are related to each controller. In order to provide a differentiation in both designs, we define (8) which establishes the control signal u_c for the conventional SMC.

$$u_c = u_{eq\_c} + u_{sw\_c} \tag{8}$$

According to authors of [48], the equivalent control term can be deduced from the statement $\dot{S}_1 = 0$. The usage of (7) allows us to obtain the following expression.

$$u_{eq\_c} = 1 - \frac{V_s}{V_o} - \frac{\lambda \cdot e \cdot L}{V_o} \tag{9}$$

On the other hand, the switching term for this case is defined by (10), based on the Ref. [49].

$$u_{sw\_c} = -k_0 \cdot sign(S_1) \tag{10}$$

Such that $k_0 > 0$ and its choice is significant because a small value can increase the response time; oppositely, strong oscillations can occur. These effects can excite neglected dynamics (chattering phenomenon), or even deteriorate the hardware [50].

3.2. Integral terminal sliding mode control

An integral terminal sliding surface S_2 is proposed as the following mathematical expression [51].

$$S_2 = e + \lambda \left(\int e\, dt\right)^{p/q} \tag{11}$$

Where the terms p and q are odd numbers which should satisfy the relation $1 < p/q < 2$ and $\lambda > 0$. The derivation of (11) leads to the following Eq. (12).

$$\dot{S}_2 = \dot{e} + \lambda \left(\frac{p}{q}\right) \cdot e \cdot \left(\int e\, dt\right)^{p/q-1} \tag{12}$$

Since the current reference is constant, therefore we define the derivative of the error as $\dot{e} = \dot{I}_L$, which is expressed in (2). Thus, $\dot{S}_2$ is declared as:

$$\dot{S}_2 = \frac{V_o}{L} u - \frac{V_o}{L} + \frac{V_s}{L} + \lambda \left(\frac{p}{q}\right) \cdot e \cdot \left(\int e\, dt\right)^{p/q-1} \tag{13}$$

The embodiment of the control law through means of an ITSMC yields to the following expression:

$$u_{int} = u_{eq\_int} + u_{sw\_int} \tag{14}$$

Where the equivalent term u_{eq_it} is gathered by $\dot{S}_2 = 0$ and it is gleaned as follows:

$$u_{eq\_int} = 1 - \frac{V_s}{V_o} - \frac{\lambda\, e\, L}{V_o} \left(\frac{p}{q}\right) \cdot \left(\int e\, dt\right)^{p/q-1} \tag{15}$$

The switching term is analogue to (10) where the proportional constant is distinguishable by k_1 which belongs to the ITSMC approach.

$$u_{sw\_int} = -k_1 \cdot sign(S_2) \tag{16}$$

3.3. Global integral terminal sliding mode control

Similarly as previous presented, in this case we define the surface as S_3 which is a global terminal integral approach.

$$S_3 = e + \alpha \int_0^t e.dt + \lambda \left(\int_0^t e.dt \right)^{p/q} \tag{17}$$

Therefore, we derive (17) and we obtained the following (18) with the subsequent replacement of (2) in the derivative of S_3.

$$\dot{S}_3 = \dot{e} + \alpha \cdot e + \lambda \left(\frac{p}{q} \right) \cdot e \cdot \left(\int_0^t e.dt \right)^{\frac{p-q}{q}} \tag{18}$$

$$\dot{S}_3 = \frac{u_c}{L}.V_o - \frac{1}{L}.V_o + \alpha \cdot e + \frac{1}{L}.V_s + \lambda \left(\frac{p}{q} \right) \cdot e \cdot \left(\int_0^t e.dt \right)^{\frac{p-q}{q}} \tag{19}$$

Like in the preceding sections, the control composition is obtained and differentiated within the following expression with its sub-indexes that corresponds to the GITSMC.

$$u_{\_git} = u_{eq\_git} + u_{sw\_git} \tag{20}$$

We retrieved the equivalent term u_{eq_git} through $\dot{S}_3 = 0$ and it is reached as follows:

$$u_{eq\_git} = 1 - \frac{V_s}{V_o} - \frac{\alpha \cdot e \cdot L}{V_o} - \frac{\lambda.e.L}{V_o} \left(\frac{p}{q} \right) \cdot \left(\int_0^t e.dt \right)^{\frac{p-q}{q}} \tag{21}$$

In regards to the switching term u_{sw_git}, the expression is similar to the mentioned sliding controllers but, the proportional constant is now replaced with a variable which is also known as QRL.

$$u_{sw\_git} = -\psi \cdot sign(S_3) \tag{22}$$

$$\psi = -\left[k_2 \left(b^{|S_3|} - 1 \right) + k_3 |S_3|^a + (D + \eta) \right] \tag{23}$$

The aim of the QRL is to improve the performance of the designed control; this comprises a similarity within the fast and double power reaching law which behaviour takes into account that the approach speed is reduced when the states are near the sliding surface so that not only enhance the rate convergence but also the chattering is moderated [52]. The parameters should adhere to the following conditions: $b > 1$, $\eta > 0$, $|S_1|^a > 1$, $k_{2,3} > 0$. The parameter D is the disturbance boundary such that $|d| \leq D$ where d is the uncertainty.

3.4. Lyapunov stability proof of CSMC, ITSMC and GITSMC

The Lyapunov stability theorem declares that a dynamical system can be asymptotically stable provided that a function (also called as *Lyapunov Function*) V(S) is positive definite and accomplishes the following conditions: $V(\infty) = \infty$, $V(0) = 0$ and $\dot{V}(S) < 0$. For all control strategies, the Lyapunov function chosen is a quadratic like (24) shows.

$$V(S) = \frac{1}{2} S^2 \tag{24}$$

$$\dot{V}(S) = S \cdot \dot{S} \tag{25}$$

Therefore, for the first case where we used a conventional SMC and by replacing S by $\dot{S}_1$ from (7), we obtained the following stability proof . The mathematical conclusion states that for the controller chosen, the system will be asymptotically stable.

$$\begin{aligned}
\dot{V}(S_1) &= S_1 \dot{S}_1 \\
&= S_1 \left[\frac{V_o}{L} u - \frac{V_o}{L} + \frac{V_s}{L} + \lambda \cdot e \right] \\
&= S_1 \left[\frac{V_o}{L} (u_{eq_c} + u_{sw_c}) - \frac{V_o}{L} + \frac{V_s}{L} + \lambda \cdot e \right] \\
&= S_1 \left[\frac{V_o}{L} u_{eq_c} + \frac{V_o}{L} u_{sw_c} - \frac{V_o}{L} + \frac{V_s}{L} + \lambda \cdot e \right] \\
&= S_1 \left[\frac{V_o}{L} \left(1 - \frac{V_s}{V_o} - \frac{\lambda \cdot e \cdot L}{V_o} \right) + \frac{V_o}{L} \left(-k_0 \cdot sign(S_1) \right) \right. \\
&\quad \left. - \frac{V_o}{L} + \frac{V_s}{L} + \lambda \cdot e \right] \\
&= -k_0 \cdot \frac{V_o}{L} \cdot S_1 \cdot sign(S_1) \\
&= -k_0 \cdot \frac{V_o}{L} \cdot |S_1| \\
&\leq 0
\end{aligned} \tag{26}$$

On the other hand, based on the ITSMC, we replaced the S in the Lyapunov function is S_2 and its derivative. On the same manner, we obtained the following stability calculation where it can also be seen that the controlled system is asymptotically stable.

$$\begin{aligned}
\dot{V}(S_2) &= S_2 \dot{S}_2 \\
&= S_2 \left[\dot{e} + \lambda \left(\frac{p}{q} \right) \cdot e \cdot \left(\int_0^t e\, dt \right)^{p/q-1} \right] \\
&= S_2 \left[u \frac{V_o}{L} - \frac{V_o}{L} + \frac{V_s}{L} + \lambda \left(\frac{p}{q} \right) \cdot e \cdot \left(\int_0^t e\, dt \right)^{p/q-1} \right] \\
&= S_2 \left[(u_{eq_rl} + u_{sw_rl}) \frac{V_o}{L} - \frac{V_o}{L} + \frac{V_s}{L} \right. \\
&\quad \left. + \lambda \left(\frac{p}{q} \right) \cdot e \cdot \left(\int_0^t e\, dt \right)^{p/q-1} \right] \\
&= S_2 \left[\frac{V_o}{L} \left(1 - \frac{V_s}{V_o} - \frac{\lambda\, e\, L}{V_o} \left(\frac{p}{q} \right) \cdot \left(\int_0^t e\, dt \right)^{p/q-1} \right. \right. \\
&\quad \left. \left. + \frac{V_o}{L} \left(-k_1 \cdot sign(S_2) \right) \right) \right] \\
&\quad + S_2 \left[-\frac{V_o}{L} + \frac{V_s}{L} + \lambda\, e \left(\frac{p}{q} \right) \cdot \left(\int_0^t e\, dt \right)^{p/q-1} \right] \\
&= -k_1 \cdot \frac{V_o}{L} \cdot S_2 \cdot sign(S_2) \\
&= -k_1 \cdot \frac{V_o}{L} \cdot |S_2| \\
&\leq 0
\end{aligned} \tag{27}$$

Lastly, we also retrieved the stability proof of the GITSMC with the QRL in the same way through a replacement of S_3 as follows.

$$\begin{aligned}
\dot{V}(S_3) &= S_3 \dot{S}_3 \\
&= S_3 \left(\frac{u_c}{L}.V_o - \frac{1}{L}.V_o + \frac{1}{L}.V_s + \alpha \cdot e \right. \\
&\quad \left. + \lambda \left(\frac{p}{q} \right) \cdot e \cdot \left(\int_0^t e.dt \right)^{p/q-1} \right) \\
&= S_3 \left(\frac{(u_{eq_git} + u_{sw_git})}{L}.V_o - \frac{1}{L}.V_o + \frac{1}{L}.V_s + \alpha \cdot e \right. \\
&\quad \left. + \lambda \left(\frac{p}{q} \right) \cdot e \cdot \left(\int_0^t e.dt \right)^{p/q-1} \right) \\
&= S_3 \left(\frac{V_o}{L} \left[1 - \frac{V_s}{V_o} - \frac{\alpha \cdot e \cdot L}{V_o} \right. \right. \\
&\quad \left. \left. - \frac{\lambda.e.L}{V_{out}} \left(\frac{p}{q} \right) \cdot \left(\int_0^t e.dt \right)^{p/q-1} - k.sign(S_3) \right] \right) \\
&\quad + S_3 \left(-\frac{1}{L}.V_o + \frac{1}{L}.V_s + \alpha \cdot e + \lambda \left(\frac{p}{q} \right) \cdot e \cdot \left(\int_0^t e.dt \right)^{p/q-1} \right) \\
&= -k \cdot \frac{V_o}{L} \cdot S_3 \cdot sign(S_3) \\
&= -k \cdot \frac{V_o}{L} \cdot |S_3| \\
&\leq 0
\end{aligned} \tag{28}$$

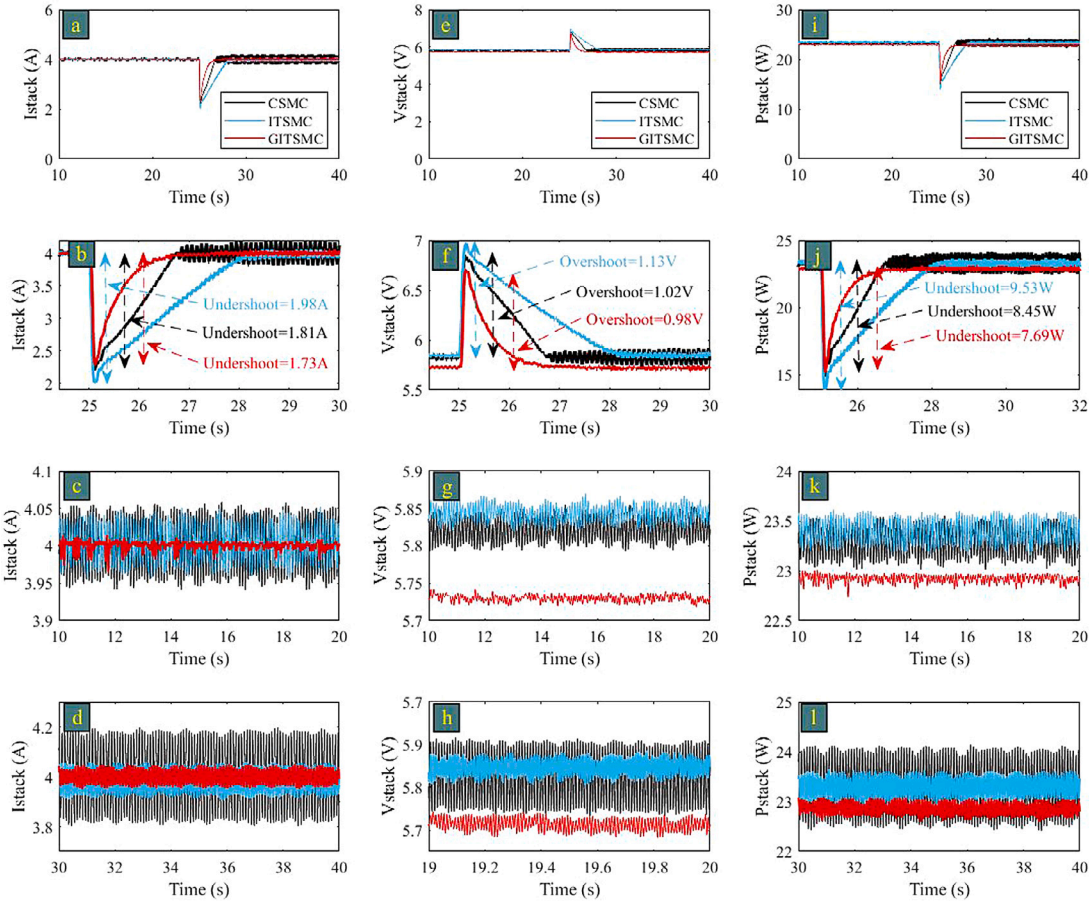

Fig. 2. Effect of increasing the load resistance. a–d: PEMFC stack current; e–h: PEMFC stack voltage; i–l: PEMFC stack power.

4. Results

In the following descriptions, we performed an in-depth analysis of the results gathered in terms of constant references and dynamical changes in the load. The tuned control parameters that we obtained through the minimization of the IAE are the following: $a = 0.2$, $b = 1.35$, $k_0 = 0.05$, $k_1 = 0.02$, $k_2 = 0.2$, $k_3 = 0.07$, $D = 1$, $\eta = 0.5$, $p = 1$, $q = 3$, $\alpha = 0.1$, $\lambda = 0.1$. The enquiry of the controllers was performed through load variations which were established as a squared according to the following specifications:

4.1. Resistance increment from 20 Ω to 50 Ω at 25 s

The electrical stack measures like I_{stack}, V_{stack} and P_{stack} are exposed in Fig. 2 where several features deserve to be highlighted. Fig. 2(b) shows the PEMFC generated current where the robustness can be reflected in the undershoot measured in the first load rise. In comparison to the ITSMC (which performance was the lowest one in this step), the SMC undershoot current was 1.81 A which entails a difference of 9.4% but the GITSMC boosted this change since the peak was 1.73 A, which is 14.5% in respect to the ITSMC. A similar trend was observed in Figs. 2(f) and (j) where V_{stack} and P_{stack} were measured and the SMC still had a better demeanour than the ITSMC since it showed the same improved features as the voltage overshoot decreased from 1.13 V to 1.02 V (near 10.8%) and the power undershoot climbed from 9.53 W to 8.45 W (around 12.8%). Nevertheless, the progress was higher with the GITSMC because of the overshoot in the voltage which difference in terms of the ITSMC dropped to 0.98 V (near 15.3%); the power exhibits the same enhancement since the overshoot declined to 7.69 W, this implies 24%. Regarding the response time for each stack analysed variable, certainly the SMC is faster than the ITSMC as the integral reduces the speed; however, the advanced GITSMC with the inclusion of the QRL could improve this feature and allowed a more active response in comparison to the other structures.

Before the first load change (at 25 s), the role of the controller was to follow a constant reference where it was possible to evaluate the chattering that each configuration developed. At the first level-off, the I_{stack} from Fig. 2(c) shows that the ITSMC increased its effectiveness with the inclusion of the integral term which was reflected in the amplitude reduction where in comparison with the SMC, it outcame an average of 33%. However, this difference increased drastically with the GITSMC as the value was augmented to 6 times. The stack voltage behaved similarly since in Fig. 2(g), the ITSMC provided an improvement of 71.8% of difference in chattering in terms of the SMC; but furthermore, the GITSMC generated a variation of 4 times higher in this feature. The stack power from Fig. 2(k) is akin to previous analysis as the SMC manages the chattering in the same low performance and thus, the ITSMC had a discrepancy of 31% whereas the GITSMC still lead this trend with 3.22 times lower amplitude.

Nevertheless between 25 and 45 s, a steady resistance of 50 Ω was settled as a constant reference following scenario where the role of each variable had considerable disparity. For instance, the SMC had the weaker performance as it provided nearly the same chattering manner where the stack current of the ITSMC developed an amplitude which was 2 times lower than the SMC but even at this point, the GITSMC had a 3 times lower amplitude. The voltage persisted with a meager performance response with the SMC and in terms of chattering, the amplitude for the ITSMC reached 72% of difference; again, the GITSMC was near 4 times. Despite that the SMC retained the equivalent behaviour as previously, the discrepancy within the ITSMC was higher since it reached 2.23 times lower amplitude; the GITSMC also achieved a superior difference with 4.6 times.

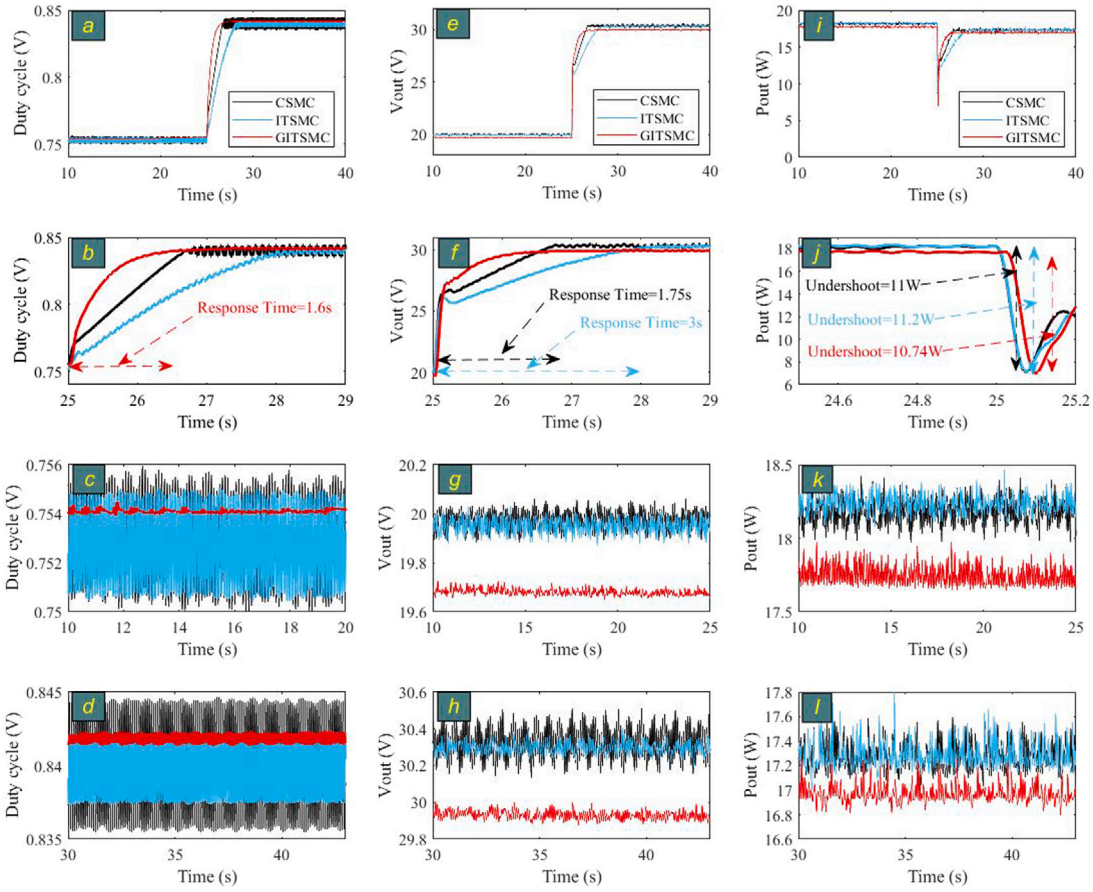

Fig. 3. Effect of increasing the load resistance. a–d: Duty cycle signal; e–h: DC–DC output voltage; i–l: DC–DC output power.

Fig. 3 exposes the performance of the duty cycle and output measures like voltage (V_{out}) and power (P_{out}) in the first load change. The proposed controllers indicated a smooth and gradual rise to the desired operating point as it can be seen through the Figs. 3(a, b, e and f). As previously in the stack variables analysis, the response time of the ITSMC is still the lowest one whereas the GITSMC displays a brisk reaction in the duty cycle as in the output voltage. Despite that the undershoot analysis of the output power in Fig. 3(j) presents a slight dissimilarity within each structure, the SMC accomplished 11.2 W and the GITSMC got a further difference with 10.74 W; referred to the 11.2 W that the ITSMC provided, the SMC and the GITSMC attained respectively, 1.8% and 4.2%. Additionally, the duty cycle from Figs. 3(c–d) show several chattering behaviour in the steady reference following. Since the duty cycle is the control action, certainly it will reflect this phenomenon in the output voltage and power as it can be seen in Figs. 3(g–h, k–l).

Experiments revealed that the performance of the PEMFC was lower than the one declared by the manufacturer. A key reason of this deterioration is the usage since the device was involved in several projects in the last 3 years. Therefore, the declared maximum output power of 50 W it was found to be 30 W. Another significant factor that was evident in the practice it is an only visible temperature effect in uncontrolled variables since the current was the main one to be tracked. For example, in Figs. 2(g–h, k–l) a slight gap is distinguished between the signals. The nature of this is caused by the temperature change inside the fuel cell which influence in the generated voltage and output power.

4.2. Resistance reduction from 50 Ω to 20 Ω at 45 s

Last description takes into account Fig. 4 which represents the analysis of the stack variables and the duty cycle when the load shifts back to 20 Ω at 45 s. The lead performance of the GITSMC, which was formerly appreciated in the first load variation, now provided the lower overshoot value with 2.8 A. Additionally, the SMC managed in like manner as it reached a peak of 3.5 A, and thus, in comparison with the ITSMC that achieved 4.25 A: the SMC improved 21.4% and the GITSMC reached 52%. This implies the performance climbs when the load is reduced and moreover, the robustness of the GITSMC is still superior. In addition, the tendency was the equally with the voltage since the SMC settled an undershoot of 1.75 V and the GITSMC even lower at 1.2 V and in terms of the 2.07 V from the ITSMC, respectively, the difference is 18.3% and 72.5%. In regards to the power, the ITSMC produced the higher value with 8.9 W whereas the SMC acquired 7.9 W and but the GITSMC increased this difference to 4.6 W; as regards to the SMC, the ITSMC enhanced the response by 12.7% and the GITSMC up to 93.5%. The stack variables established that the GITSMC developed a better performance, and besides, along Figs. 4(b, d, f) it can be seen that this advanced structure also carries with the best time response.

The control action in Fig. 4(h) indicates the response time of each controller with a modest discrepancy to the analysed trend where the SMC drove with the advantage of 1.7 s over the 3.3 s that corresponds to the ITSMC, which is a difference of 94.4%; in this case, the GITSMC reduced its performance because the response time is 1.9 s, which implies 73% less than the ITSMC. Nevertheless, the GITSMC rebounded to previous trend in the output voltage where an undershoot of 2.8 V represented 78.5% lower than the 5 V of the ITSMC; in the same way, the SMC had a small variance with 3.8 V, which is 31.5% in terms of the ITSMC. The output power, similarly to the first rise at 25 s, displayed again a modest difference where the ITSMC had the highest overshoot value with 17.5 W followed by the SMC that declined to 17.4 W (around 0.5%) and finally the GITSMC performed better with 17 W (near 3%).

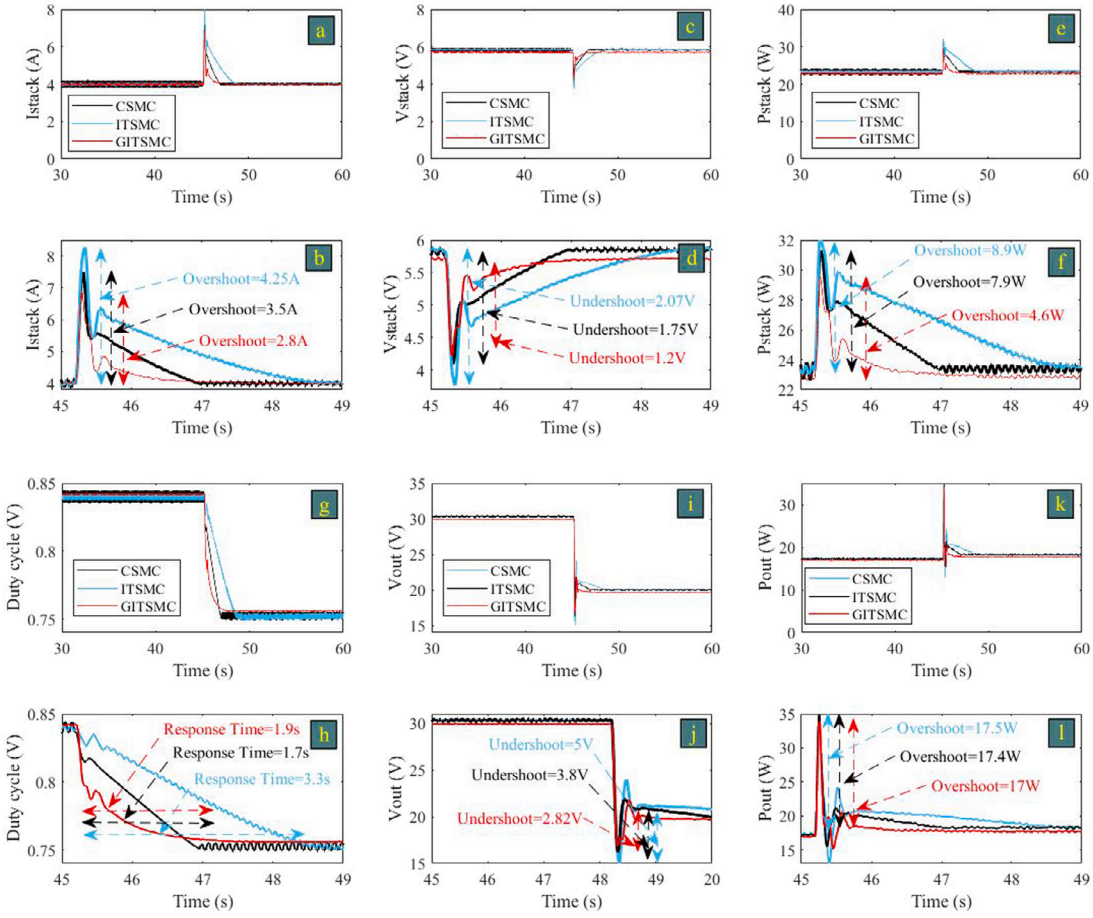

Fig. 4. Effect of decreasing the load resistance. a–b: PEMFC stack current; c–d: PEMFC stack voltage; e–f: PEMFC stack power; g–h: Duty cycle signal; i–j: DC–DC output voltage; k–l: DC–DC output power.

5. Conclusions

In this research, an innovative structure for current reference following was defined and embedded in a proton exchange membrane fuel cell. Advance controllers like sliding mode control and integral terminal sliding mode control were also implemented and contrasted with the novel design to highlight the features that could define the effectiveness of each in different scenarios such as constant and dynamic change following.

An assembled test rig with a commercial Heliocentris fuel cell linked to a boost converter were used to evaluate each structure in a dSpace DS1102. The device can be controlled through a pulse-width-modulation signal generator that belongs to the converter, and this was managed by a proper designed controller. The reference was established as two load changes at 25 s and 45 s where in the first one, the resistance shifted from 20 Ω to 50 Ω and in the second step regressed to 20 Ω.

Experimental results showed that during the dynamic changes, the global integral terminal sliding mode controller had the superior performance as in terms of robustness since the overshoot and undershoot values are better than the compared controllers. Followed by this in terms of effectiveness, the sliding mode control also demonstrated that it could gather a remarkable behaviour contrasted with the integral terminal sliding mode control. However, results changed when a constant reference had to be followed since the integral terminal sliding mode controller had less chattering than the conventional sliding mode controller. Nevertheless, the global integral terminal sliding mode controller maintained the outstanding trend even in this case which proved to be a suitable controller yet in terms of reduction of energy consumption. Finally, the application of this control scheme has been corroborated in a real time experimental validation over a commercial proton exchange membrane fuel cell.

CRediT authorship contribution statement

Cristian Napole: Conceptualization, Methodology, Formal analysis, Investigation, Writing – original draft, Writing – review & editing, Visualization. **Mohamed Derbeli:** Methodology, Software, Validation, Investigation, Data curation, Writing – review & editing. **Oscar Barambones:** Investigation, Writing – review & editing, Supervision, Project Administration, Funding acquisition.

Acknowledgements

The authors wish to express their gratitude to the Basque Government, through the project EKOHEGAZ (ELKARTEK KK-2021/00092), to the Diputación Foral de Álava (DFA), through the project CONAVANTER, and to the UPV/EHU, through the project GIU20/063, for supporting this work.

References

[1] Smith AM, Ross AB. Production of bio-coal, bio-methane and fertilizer from seaweed via hydrothermal carbonisation. Algal Res 2016;16:1–11. http://dx.doi.org/10.1016/j.algal.2016.02.026.

[2] Guerra O, Eichman J, Kurtz J, Hodge B-M. Cost competitiveness of electrolytic hydrogen. Joule 2019;3. http://dx.doi.org/10.1016/j.joule.2019.07.006.

[3] Zakaria Z, Kamarudin S, Timmiati S. Membranes for direct ethanol fuel cells: An overview. Appl Energy 2016;163:334–42. http://dx.doi.org/10.1016/j.apenergy.2015.10.124.

[4] Ho J, Saw E-C, Lu L, Liu J. Technological barriers and research trends in fuel cell technologies: A citation network analysis. Technol Forecast Soc Change 2014;82:66–79. http://dx.doi.org/10.1016/j.techfore.2013.06.004.

[5] Weidner E, Cebolla RO, Davies J. Global deployment of large capacity stationary fuel cells. JRC technical reports, 2019, http://dx.doi.org/10.2760/372263.

[6] Wilberforce T, Ijaodola O, Ogungbemi E, Hassan ZE, Thompson J, Olabi AG. Effect of bipolar plate materials on performance of fuel cells. In: Reference module in materials science and materials engineering. Elsevier; 2018, http://dx.doi.org/10.1016/B978-0-12-803581-8.11272-X.

[7] Yonoff RE, Ochoa GV, Cardenas-Escorcia Y, Silva-Ortega JI, no Stand LM. Research trends in proton exchange membrane fuel cells during 2008–2018: A bibliometric analysis. Heliyon 2019;5(5):e01724. http://dx.doi.org/10.1016/j.heliyon.2019.e01724.

[8] Kurnia JC, Chaedir BA, Sasmito AP, Shamim T. Progress on open cathode proton exchange membrane fuel cell: Performance, designs, challenges and future directions. Appl Energy 2021;283:116359. http://dx.doi.org/10.1016/j.apenergy.2020.116359.

[9] Mayyas A, Mann M. Emerging manufacturing technologies for fuel cells and electrolyzers. Procedia Manuf 2019;33:508–15. http://dx.doi.org/10.1016/j.promfg.2019.04.063.

[10] Feng Y, Dong Z. Integrated design and control optimization of fuel cell hybrid mining truck with minimized lifecycle cost. Appl Energy 2020;270:115164. http://dx.doi.org/10.1016/j.apenergy.2020.115164.

[11] Sankar K, Aguan K, Jana AK. A proton exchange membrane fuel cell with an airflow cooling system: Dynamics, validation and nonlinear control. Energy Convers Manage 2019;183:230–40. http://dx.doi.org/10.1016/j.enconman.2018.12.072.

[12] Gerbec M, Jovan V, Petrovčič J. Operational and safety analyses of a commercial PEMFC system. Int J Hydrogen Energy 2008;33(15):4147–60. http://dx.doi.org/10.1016/j.ijhydene.2008.04.063.

[13] Li Q, Wang T, Li S, Chen W, Liu H, Breaz E, et al. Online extremum seeking-based optimized energy management strategy for hybrid electric tram considering fuel cell degradation. Appl Energy 2021;285:116505. http://dx.doi.org/10.1016/j.apenergy.2021.116505.

[14] Gu J, Abbas G, Samad A, Asad MU, Farooq U. Set-point tracking of a DC-DC boost converter through optimized PID controllers. In: 2016 IEEE Canadian conference on electrical and computer engineering. 2016, p. 1–5. http://dx.doi.org/10.1109/CCECE.2016.7726841.

[15] Alharbi B, Alhomim M, McCann R. Robust control of DC-DC boost converter by using μ -synthesis approach. IFAC-PapersOnLine 2019;52(4):200–5. http://dx.doi.org/10.1016/j.ifacol.2019.08.261.

[16] Habib M, Khoucha F, Harrag A. GA-based robust LQR controller for interleaved boost DC–DC converter improving fuel cell voltage regulation. Electr Power Syst Res 2017;152:438–56. http://dx.doi.org/10.1016/j.epsr.2017.08.004.

[17] Derbeli M, Farhat M, Barambones O, Sbita L. Control of PEM fuel cell power system using sliding mode and super-twisting algorithms. Int J Hydrogen Energy 2017;42(13):8833–44. http://dx.doi.org/10.1016/j.ijhydene.2016.06.103.

[18] Quan S, Wang Y-X, Xiao X, He H, Sun F. Feedback linearization-based MIMO model predictive control with defined pseudo-reference for hydrogen regulation of automotive fuel cells. Appl Energy 2021;293:116919. http://dx.doi.org/10.1016/j.apenergy.2021.116919.

[19] Benchouia NE, Derghal A, Mahmah B, Madi B, Khochemane L, Hadjadj Aoul E. An adaptive fuzzy logic controller (AFLC) for PEMFC fuel cell. Int J Hydrogen Energy 2015;40(39):13806–19. http://dx.doi.org/10.1016/j.ijhydene.2015.05.189.

[20] Safwat IM, Wu X, Zhao X, Li W. Adaptive fuzzy logic control of boost converter fed by stand-alone PEM fuel cell stack. In: 2017 IEEE transportation electrification conference and expo, asia-pacific. 2017, p. 1–6. http://dx.doi.org/10.1109/ITEC-AP.2017.8080956.

[21] Broesch JD. Applications of DSP. In: Broesch JD, editor. Digital signal processing. Burlington: Newnes; 2009, p. 125–34. http://dx.doi.org/10.1016/B978-0-7506-8976-2.00007-9, Chapter 7.

[22] Fang F, Wei L. Backstepping-based nonlinear adaptive control for coal-fired utility boiler–turbine units. Appl Energy 2011;88(3):814–24. http://dx.doi.org/10.1016/j.apenergy.2010.09.003.

[23] Derbeli M, Barambones O, Lassaad S. A robust maximum power point tracking control method for a PEM fuel cell power system. Appl Sci 2018;8:2449. http://dx.doi.org/10.3390/app8122449.

[24] Nizami TK, Chakravarty A. Neural network integrated adaptive backstepping control of DC-DC boost converter. IFAC-PapersOnLine 2020;53(1):549–54. http://dx.doi.org/10.1016/j.ifacol.2020.06.092.

[25] Cao L, Shengxiu Z, Xiaofeng L, Yinan L, Ying L. Nonlinear adaptive block backstepping control using command filter and neural networks approximation. Inform Technol J 2011;10:2284–91. http://dx.doi.org/10.3923/itj.2011.2284.2291.

[26] Coban R. Backstepping integral sliding mode control of an electromechanical system. Automatika 2017;58:266–72. http://dx.doi.org/10.1080/00051144.2018.1426263.

[27] Sankar K, Jana AK. Dynamics and estimator-based nonlinear control of a PEM fuel cell. IEEE Trans Control Syst Technol 2018;26(3):1124–31. http://dx.doi.org/10.1109/TCST.2017.2695165.

[28] Ziogou C, Voutetakis S, Georgiadis M, Papadopoulou S. Model predictive control (MPC) strategies for PEM fuel cell systems: A comparative experimental demonstration. Chem Eng Res Des 2018;131. http://dx.doi.org/10.1016/j.cherd.2018.01.024.

[29] Hausberger T, Kugi A, Eder A, Kemmetmüller W. High-speed nonlinear model predictive control of an interleaved switching DC/DC-converter. Control Eng Pract 2020;103:104576. http://dx.doi.org/10.1016/j.conengprac.2020.104576.

[30] Yang S, Wan MP, Chen W, Ng BF, Dubey S. Experiment study of machine-learning-based approximate model predictive control for energy-efficient building control. Appl Energy 2021;288:116648. http://dx.doi.org/10.1016/j.apenergy.2021.116648.

[31] Wang B, Ma G, Xu D, Zhang L, Zhou J. Switching sliding-mode control strategy based on multi-type restrictive condition for voltage control of buck converter in auxiliary energy source. Appl Energy 2018;228:1373–84. http://dx.doi.org/10.1016/j.apenergy.2018.06.141.

[32] Yin L, Turesson G, Tunestål P, Johansson R. Sliding mode control on receding horizon: Practical control design and application. Control Eng Pract 2021;109:104724. http://dx.doi.org/10.1016/j.conengprac.2021.104724.

[33] Gambhire S, Kishore D, Londhe P, Pawar S. Review of sliding mode based control techniques for control system applications. Int J Dyn Control 2021;9. http://dx.doi.org/10.1007/s40435-020-00638-7.

[34] Zak M. Terminal attractors in neural networks. Neural Netw 1989;2(4):259–74. http://dx.doi.org/10.1016/0893-6080(89)90036-1.

[35] Venkataraman ST, Gulati S. Control of nonlinear systems using terminal sliding modes. In: 1992 American control conference. 1992, p. 891–3. http://dx.doi.org/10.23919/ACC.1992.4792209.

[36] Levant A, Pridor A, Gitizadeh R, Yaesh I, Ben Asher J. Aircraft pitch control via second-order sliding technique. J Guid Control Dyn 2000;23:586–94. http://dx.doi.org/10.2514/2.4591.

[37] Napole C, Barambones O, Derbeli M, Calvo I, Silaa M, Velasco J. High-performance tracking for piezoelectric actuators using super-twisting algorithm based on artificial neural networks. Mathematics 2021;9:244. http://dx.doi.org/10.3390/math9030244.

[38] Deepika D, Kaur S, Narayan S. Integral terminal sliding mode control unified with UDE for output constrained tracking of mismatched uncertain non-linear systems. ISA Trans 2020;101:1–9. http://dx.doi.org/10.1016/j.isatra.2020.01.002.

[39] Morshed M, Fekih A. Design of a chattering-free integral terminal sliding mode approach for DFIG-based wind energy systems. Optim Control Appl Methods 2020;1–17. http://dx.doi.org/10.1002/oca.2635.

[40] Armghan H, Yang M, Armghan A, Ali N, Wang M, Ahmad I. Design of integral terminal sliding mode controller for the hybrid AC/DC microgrids involving renewables and energy storage systems. Int J Electr Power Energy Syst 2020;119:105857. http://dx.doi.org/10.1016/j.ijepes.2020.105857.

[41] Chiu C-S, Shen C-T. Finite-time control of DC–DC buck converters via integral terminal sliding modes. Int J Electron 2012;99:643–55. http://dx.doi.org/10.1080/00207217.2011.643493.

[42] Xiu C, Guo P. Global terminal sliding mode control with the quick reaching law and its application. IEEE Access 2018;6:49793–800. http://dx.doi.org/10.1109/ACCESS.2018.2868785.

[43] Pan H, Zhang G, Ouyang H, Mei L. A novel global fast terminal sliding mode control scheme for second-order systems. IEEE Access 2020;8:22758–69. http://dx.doi.org/10.1109/ACCESS.2020.2969665.

[44] Ventura UP, Fridman L. Chattering measurement in SMC and hosmc. In: 2016 14th international workshop on variable structure systems. 2016, p. 108–13. http://dx.doi.org/10.1109/VSS.2016.7506900.

[45] Eker I. Second-order sliding mode control with experimental application. ISA Trans 2010;49(3):394–405. http://dx.doi.org/10.1016/j.isatra.2010.03.010.

[46] Slotine J, Li W. Sliding surfaces. In: Applied nonlinear control. Prentice Hall; 1991, p. 278–9, Ch..

[47] Bahrami M, Ebrahimi B, Ansarifar G. Sliding mode observer and control design with adaptive parameter estimation for a supersonic flight vehicle. Int J Aerosp Eng 2010;2010:9. http://dx.doi.org/10.1155/2010/474537.

[48] Derbeli M, Barambones O, Farhat M, Ramos-Hernanz JA, Sbita L. Robust high order sliding mode control for performance improvement of PEM fuel cell power systems. Int J Hydrogen Energy 2020;45(53):29222–34. http://dx.doi.org/10.1016/j.ijhydene.2020.07.172.

[49] Silaa M, Derbeli M, Barambones O, Napole C, Cheknane A, Durana J. An efficient and robust current control for polymer electrolyte membrane fuel cell power system. Sustainability 2021;13. http://dx.doi.org/10.3390/su13042360.

[50] Fridman L, Moreno J, Iriarte R. Sliding modes after the first decade of the 21st century: State of the art, Vol. 412. 2011, p. 11–2. http://dx.doi.org/10.1007/978-3-642-22164-4.

[51] Xu D, Liu Q, Yan W, Yang W. Adaptive terminal sliding mode control for hybrid energy storage systems of fuel cell, battery and supercapacitor. IEEE Access 2019;7:29295–303. http://dx.doi.org/10.1109/ACCESS.2019.2897015.

[52] Zhao Y, Wu T, Ma Y. A double power reaching law of sliding mode control based on neural network. Math Probl Eng 2013;2013. http://dx.doi.org/10.1155/2013/408272.